ARTICLES

Role of Surface Relaxation in the Eley−Rideal Formation of H_2 on a Graphite Surface†

S. Morisset, F. Aguillon,* M. Sizun, and V. Sidis

Laboratoire des Collisions Atomiques et Moléculaires, Unité Mixte de Recherche CNRS et Université Paris-Sud UMR 8625, Fédération de Recherche "Lumière Matière" FR 2764, Bât 351, Université de Paris-Sud, F91405 Orsay Cedex, France

Received: January 3, 2004; In Final Form: April 8, 2004

A wave packet study of the dynamics of H_2 formation through a collinear Eley−Rideal mechanism that explicitly handles the substrate relaxation effects is presented. The substrate used is a planar PAH which exhibits some strong similarities with a perfect graphite (0001) surface. The collision energy range investigated lies between 0.4 meV ($T = 5$ K) and 0.46 eV. The reaction probability is large, except at very low collision energy. Most of the available energy goes into the H_2 vibration, which is much more excited than the substrate. Focusing on the surface relaxation effects, the results are compared with two widely used approximations, namely, the sudden approximation and the adiabatic approximation.

1. Introduction

It is now commonly admitted that the formation of molecular hydrogen in cold clouds of the interstellar medium (ISM) proceeds through a chemical reaction at the surface of interstellar dust grains.[1] Three mechanisms are generally invoked: in the Eley−Rideal (ER) mechanism, an H atom, initially adsorbed on the surface, is hit by the second H atom from the gas phase, leading to a fast reaction. In the Langmuir−Hinshelwood (LH) mechanism, both H atoms are initially adsorbed on the surface. During their diffusion on the surface, they can meet together and eventually recombine and desorb. Finally, the hot atom (HA) mechanism is somewhat intermediate between the ER and LH mechanisms: one of the H atoms is trapped on the surface; the second one, coming from the gas phase, is temporally trapped on the surface but reacts before its thermalisation.

The rate of these mechanisms is obviously of crucial importance as it determines the H_2/H abundance ratio in the ISM. Moreover, the amount of energy deposited by the reaction in internal and external degrees of freedom of the nascent H_2 is also important because it governs the infrared emission of the interstellar clouds.[2,3] That is the reason why in recent years a considerable amount of experimental work has been devoted to the study of H_2 formation on surfaces,[4−9] which have often been phenomenologically interpreted within the framework of the LH mechanism.[10−12] Very recently, a number of theoretical works have been undertaken, mainly to investigate the dynamics of the (ER) mechanism.[13−23] In all these works, the dust grain has been modeled by a graphite surface or a polyaromatic hydrocarbon (PAH) molecule. Indeed, although the chemical nature of the interstellar dust is not yet precisely established, there are strong indications in favor of a carbonaceous composition.[24,25]

Despite the large number of works on the subject, the problem of the formation of H_2 is far from being solved. Indeed, experimentally manipulating H atoms and determining the internal state of the H_2 molecules in the extreme conditions of the IMS ($T \approx 10$ K) is a tremendous challenge. From a theoretical point of view, an exact solution of the problem is by far out of reach of today's capabilities: the low temperature requires a very accurate description of the potential energy surface (PES); the light H atoms behave very quantally; the description of the dynamics cannot pretend to be exact without taking into account the relaxation of the grain.

Basically, three approaches have been used to determine the PES. The first approach consists of modeling the potential either by a sum of "pairwise" interactions[13,17] (e.g., H−H, H−surface), or by a London−Eyring−Polanyi−Sato (LEPS)-type PES.[14,19] In both cases, the parameters of the model are chosen to mimic the characteristics of known systems. The second approach used in our group by Sidis et al.[26,27] consists of modeling the dust grain by a PAH, namely, the coronene molecule. The PES calculation is done at the density functional theory (DFT) level. Farebrother[15] initiated the third approach, which consists of computing at the DFT level the interaction of two H atoms with a graphite surface represented by a periodic slab. The PES they obtained significantly differs from the one of Sidis.[27] This has first been attributed to the difference in the model used. Surprisingly, another DFT-PES obtained using a periodic slab calculation by Sha et al.[20] is very close to the one of Sidis[27] and thus different from Farebrother's one. One of the main differences is that the chemisorption of one H atom requires an sp^3 hybridization of the C atom involved in the graphite−H bond for both Sha's and Sidis' PES but not for Farebrother's PES. Very recently, two other groups have obtained a PES using a periodic slab at the DFT level. They also concluded that some sp^3 hybridization of the C atom is observed when H is chemisorbed.[28−30] The origin of the discrepancy between the slab DFT calculations is not elucidated. Nevertheless, as Sidis' PES is in close agreement with three of these PESs among four, we have confidently used it in the present paper.

† Part of the "Gert D. Billing Memorial Issue".

10.1021/jp049969q CCC: $27.50
Published on Web 06/10/2004

The quantal study of the ER dynamics has been undertaken in three groups. In the groups of Clary[15,16] and Jackson[18,20,21] quantal calculations have been performed in a reduced geometry where two or three degrees of freedom are considered. Recently, we have also studied the dynamics of ER reaction 1 down to very low temperature (4 K) in a quantum mechanical approach involving two degrees of freedom.[22] In the above-mentioned works, the relaxation of the surface was not taken into account. Most of them use a sudden approximation, where the surface relaxation time scale is assumed to be much longer than the reaction time; Jackson and co-workers have also used an adiabatic approximation where, on the contrary, the relaxation of the surface is assumed to be much faster than the reaction. Nevertheless, because the reaction involves a short-lived complex,[22] we have estimated that the vibration period of the carbon out of the surface plane is comparable with the collision time, namely, a few tens of femtoseconds. In such conditions, neither of the two approximations are expected to be valid.

The surface relaxation effects have only been investigated either in a purely classical framework[14,19] or a semiclassical description,[17] where the classical motion of the H atoms is coupled to the quantum bath of the phonons. The aim of the present work is to investigate the role of the surface relaxation at a quantal level. We shall examine what happens when the C atom bound to the H atom is allowed to move perpendicularly to the surface plane. The paper is organized as follows: the PES and the dynamics method are presented in sections 2 and 3, respectively. Section 4 is devoted to the results and their discussion. Section 5 gives the concluding remarks.

2. Potential

The description of the PES calculation has been done in a previous publication[27] and will only be summarized here. The graphite (0001) basal surface is simply represented by a large polycyclic aromatic hydrocarbon (PAH), namely, coronene, $C_{24}H_{12}$, hereafter denoted cor. The problem of molecular hydrogen formation then amounts to the study of the chemical reaction

$$\text{cor}-\text{H} + \text{H} \rightarrow \text{cor} + \text{H}_2 \qquad (1)$$

In coronene, the C atoms form a planar hexagonal mesh and the H atoms serve only to passivate the pending bonds of the C_{24} cluster. The calculations are done within the framework of density functional theory (DFT), using the ADF[31] computer code. The exchange-correlation density functional includes the local functional of Vosko et al.[32] and the PW91[33] generalized gradient correction. The Kohn−Sham molecular orbitals are expanded as linear combinations of atom-centered Slater-type orbitals; triple-ζ+polarization (TZP) bases have been used,[27] leading to a substantial improvement of the results with respect to the formerly published work,[26] based upon the use of double-ζ+polarization (DZP) bases. The spin polarization is allowed for by letting the spin up and spin down densities be different.

The main characteristics of the potential energy surface (PES) of the cor−H compound are the following:

(1) The H atom can be bound either in a chemisorption or a physisorption well.

(2) The equilibrium position for chemisorption is reached when the H atom is located just on top of one C atom of the coronene molecule. In the following, we shall denote this particular C atom by C*. The equilibrium distance between the H atom and the coronene plane is $2.85a_0$. The C* atom is displaced outside the coronene plane toward the H atom, $0.65a_0$ above the coronene plane. The depth of the coronene−H well is 0.44 eV; the minimum energy path (MEP) for the coronene−H association exhibits a rather high barrier (0.25 eV above the dissociation limit).

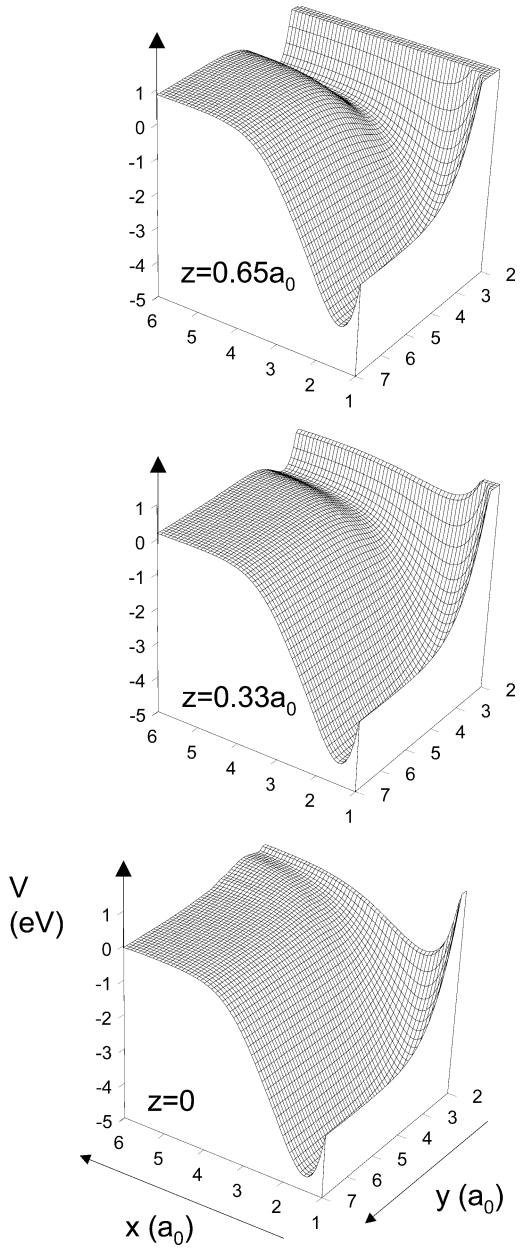

Figure 1. Cuts of the PES obtained at various values of z: $z = 0.65a_0$ is the equilibrium position of the C* atom in the cor−H molecule, $z = 0$ is the equilibrium position of the C* in the coronene molecule.

(3) The physisorption induces virtually no changes in the coronene geometry. The equilibrium cor−H distance is $7.9a_0$, and the physisorption well depth is about 8 meV. These numbers are almost independent of the site of the H atom above the coronene plane.

The work presented here corresponds to a situation where the exchanged H atom is initially in the chemisorption well. Our goal is to investigate the dynamics of reaction 1 in a time dependent framework at low temperature. As this type of calculation is computationally heavy, we have restricted ourselves to a constrained geometry: the two H atoms can move on a line perpendicular to the coronene plane, just on top of the C* atom, which belongs to the inner ring of the coronene molecule. The C* atom is also allowed to move perpendicularly to the coronene plane. Figure 1 shows some cuts of the cor−

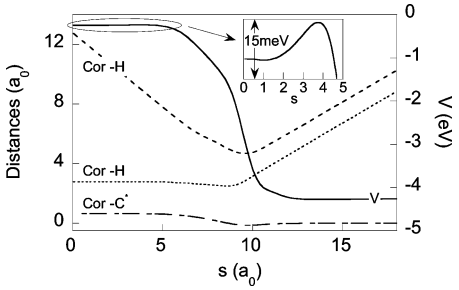

Figure 2. Minimum energy path (MEP) for the title reaction; *s* is the reaction coordinate. Full line: potential along the MEP. Dashed line and dotted line: distance between the H atoms and the coronene plane. Dash-dotted line: distance between the C* atom and the coronene plane. The inset shows the energy barrier in the entrance valley.

H−H PES obtained at fixed positions of C*. The coordinates used in this figure, and throughout this paper, are the following:

$$x = \text{H}-\text{H}, \quad y = \text{coronene plane}-\text{H}, \quad \text{and } z = \text{coronene plane}-\text{C}^* \tag{2}$$

The binding energy between the chemisorbed H atom and the coronene molecule is 0.44 eV. The binding energy of H_2 in its $v = 0$ ground state is 4.49 eV. The exoergicity of the reaction is 4.05 eV, and the H_2 molecule can be formed in its first 12 vibrational states at zero collision energy.

An important feature of the PES is the existence of a barrier in the entrance valley. This barrier is very small: when taking into account the zero-point energy of the degrees of freedom perpendicular to the minimum energy path (MEP), its height is 9.2 meV. The DFT-PES calculation is probably not precise enough to guarantee such an accuracy. Nevertheless, the same barrier has been found by different DFT-PES calculations[20,21] This barrier is seen in Figure 2, which shows the potential along the MEP as a function of the intrinsic reaction coordinates[34] defined by

$$(\mathrm{d}s)^2 = (\mathrm{d}R_{\mathrm{ms}})^2 + (\mathrm{d}r_{\mathrm{ms}})^2 + (\mathrm{d}z_{\mathrm{ms}})^2 \tag{3}$$

R_{ms} and r_{ms} are the mass-scaled Jacobi coordinates, and z_{ms} is the mass-scaled coordinate associated with the natural z coordinate:

$$R_{\mathrm{ms}} = x + y$$
$$r_{\mathrm{ms}} = y$$
$$z_{\mathrm{ms}} = \sqrt{\frac{M}{m}}z \tag{4}$$

where m (respectively, M) is the mass of an H atom (respectively, a C atom). The main advantage of this intrinsic reaction coordinate is that the kinetic energy operator associated with a motion along the MEP is simply

$$\hat{\mathrm{T}} = -\frac{\hbar^2}{2m}\frac{\partial^2}{\partial s^2} \tag{5}$$

3. Dynamics

The dynamics calculations are performed using a wave packet propagation technique. Indeed the reaction is so exoergic that the number of states which should be included in a time independent calculation is very large; in such conditions, a wave packet approach is more efficient. As we want to study the dynamics down to very low collision energy ($T < 10$ K), the typical wavelengths of the incoming wave packet are very large. Then, the size of the grid has to be made very large, which makes the calculation very time-consuming. To keep the amount of computation at a reasonable size, we have used two nonstandard features. First, as in our previous study,[22] we use the valence-like coordinates x and y. The advantage of using these coordinates is that one can very efficiently sample the region that is energetically accessible to the system using an L-shaped grid.[35] The size of the grid scales linearly with the wavelength that has to be represented. The Hamiltonian that governs the time evolution of the system is

$$\hat{\mathbf{H}} = \frac{\hat{p}_x^{\,2}}{m} + \frac{\hat{p}_y^{\,2}}{2m} - \frac{\hat{p}_x\hat{p}_y}{m} + \frac{\hat{p}_z^{\,2}}{2M} + V(x,y,z) \tag{6}$$

The volume element associated with the wave function is simply dx dy dz. Actually, form 6 of the Hamiltonian cannot be used as is, because it is not numerically hermitian. To ensure hermiticity, it has to be written in the following way[22]

$$\hat{\mathbf{H}} = \frac{\hat{p}_x(2\hat{p}_x - \hat{p}_y)}{2m} + \frac{\hat{p}_y(\hat{p}_y - \hat{p}_x)}{2m} + \frac{\hat{p}_z^{\,2}}{2M} + V(x,y,z) \tag{7}$$

Second, as the wavelength associated with the x coordinate is much larger at large x than at small x, we use a nonuniform grid spacing which samples more efficiently the phase space available to the system,[36] especially in the x direction. Efficient mapping procedures have been proposed by different groups.[37,38] Here we use the mapping procedure proposed by Borisov,[39] which is easier to implement. Technically, the idea of the mapping procedure is to introduce a new coordinate, that we shall denote x', related to x by

$$J = \frac{\mathrm{d}x}{\mathrm{d}x'} \tag{8}$$

and to use a wave function $\psi(x',y,z)$ defined by

$$\psi = \frac{\psi}{\sqrt{J}} \tag{9}$$

in such a way that the volume element associated with the new wave function ψ is simply dx' dy dz. The Hamiltonian operator that governs the time evolution of ψ is formally identical to the unmapped Hamiltonian 6:

$$\hat{\mathbf{H}} = \frac{\hat{p}_{x'}(2\hat{p}_{x'} - \hat{p}_y)}{2m} + \frac{\hat{p}_y(\hat{p}_y - \hat{p}_{x'})}{2m} + \frac{\hat{p}_z^{\,2}}{2M} + V(x',y,z) \tag{10}$$

It only differs by the expression of the linear momentum operator associated with the mapped coordinate:

$$\hat{p}_{x'} = \frac{\hbar}{\mathrm{i}}\frac{1}{\sqrt{J}}\frac{\partial}{\partial x'}\frac{1}{\sqrt{J}} \tag{11}$$

Provided the wave function ψ is equally sampled on a regular mesh in the three directions x', y, and z, the Hamiltonian is easily evaluated using the standard Fourier technique.[40] Then, the only task consists of choosing the Jacobian function J of eq 8 in such a way that a constant spacing $\delta x'$ corresponds to an adequate spacing of the grid in the x representation and then to integrate eq 8 in order to express x' as a function of x. Since the two expressions 7 and 10 of the Hamiltonian are mathematically equivalent, different J functions should yield the same physical results, although they may have very different numerical efficiencies. In the present work, J is chosen to be

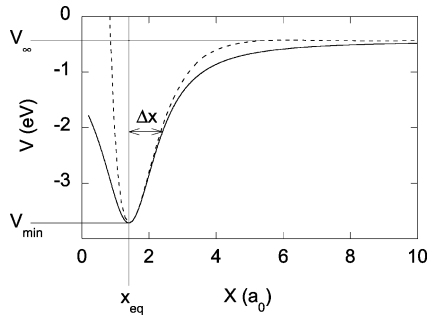

Figure 3. Full line, $V_{\text{mapping}}(x)$, as defined in eq 13. The dashed line shows the minimum of the actual potential on the whole range of y values, when the carbon atom is kept fixed at its equilibrium position in the coronene−H compound.

proportional to the de Broglie wavelength associated with an ad hoc potential $V_{\text{mapping}}(x)$ at a fictitious energy E_{mapping}:

$$J = \frac{1}{\lambda_0}\sqrt{\frac{2\pi^2\hbar^2}{m(E_{\text{mapping}} - V_{\text{mapping}}(x))}} \tag{12}$$

In the above equation, λ_0 is just a length that is formally introduced in eq 12 to ensure that J is a dimensionless number; its numerical value does not matter at all. E_{mapping} is the highest energy present in the initial wave packet. $V_{\text{mapping}}(x)$ is built analytically:

$$V_{\text{mapping}}(x) = \frac{(x - x_{\text{eq}})^2 V_\infty + \Delta x^2 V_{\text{min}}}{(x - x_{\text{eq}})^2 + \Delta x^2} \tag{13}$$

The four parameters V_{min}, V_∞, x_{eq}, and Δx are such that $V_{\text{mapping}}(x)$ is slightly smaller than the minimum of the actual potential within the whole range of y values, z being fixed at its equilibrium value in the cor−H compound (Figure 3). This choice of V_{mapping} yields a large δx grid spacing in the entrance valley, where V is large, and a small δx when the two H atoms are close together. This choice has been validated on a test 2D computation, with the z value kept fixed at $z = 0.65a_0$. It has been possible to reduce the number of grid points in the x direction typically by a factor 5, with virtually no loss of accuracy. The number of Fourier transforms needed to evaluate Hamiltonian 10 is twice what would be required to evaluate form 6 of the same Hamiltonian. That is the price to pay for the use of the mapped valence coordinate x'. This price is more than compensated by the use an L-shaped mapped grid. Altogether, the gain in numerical efficiency is estimated to be a factor 8, compared to a standard grid based on Jacobi or hyperspherical coordinates. Of course, this gain gets larger when the collision energy decreases.

The time dependent Schrödinger equation (TDSE)

$$\mathrm{i}\hbar\frac{\mathrm{d}\psi}{\mathrm{d}t} = \hat{\mathbf{H}}\psi - \mathrm{i}V_{\text{abs}}(x,y)\psi \tag{14}$$

is solved using the Lanczos algorithm.[41] The negative imaginary potential $-\mathrm{i}V_{\text{abs}}$ is added to the actual Hamiltonian operator at large values of x or y in order to avoid spurious reflections at the edges of the grid. It is defined by

$$V_{\text{abs}}(q) = \beta_q(q - q_{\text{max}} + \Delta)^3 \qquad \text{if } q > q_{\text{max}} - \Delta$$
$$V_{\text{abs}}(q) = 0 \qquad \text{if } q \le q_{\text{max}} - \Delta \tag{15}$$

where q stands for x or y, q_{max} is the value of q at the edge of the grid, and Δ is the width of the absorption zone. The initial wave packet is written

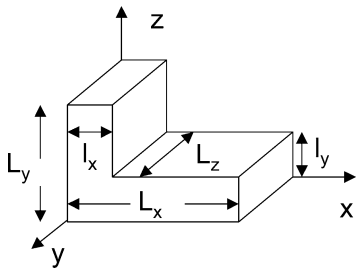

Figure 4. Shape of the grid used in the calculation.

$$\psi(R,y,z,t{=}0) = F(R)\chi_{\nu_1\nu_2}(y,z) \tag{16}$$

$\chi_{\nu_1\nu_2}$ is the vibrational eigenstate of the cor−H compound. Because in the interstellar medium this compound is always in its ground vibrational state, ν_1 and ν_2 have been set to 0. R is the Jacobi coordinate in the entrance channel ($R = x + y$), and $F(R)$ is chosen to be a Gaussian wave packet

$$F(R) = \left(\frac{1}{\pi\sigma^2}\right)^{1/4} \exp\left(-\frac{(R - R_0)^2}{2\sigma^2}\right)\exp(-\mathrm{i}K_0R) \tag{17}$$

R_0 is the initial position of the center of the wave packet; it has to be chosen large enough to ensure that the system is not in the interaction region. The energy window of the wave packet is defined by K_0 and σ. In principle, a single run could handle the whole energy domain encompassed within the initial wave packet. In practice, efficient absorption of the wave packet becomes difficult when the energy range is too broad. Then, we have covered the desired collision energy range (0.4 meV $< E_{\text{coll}} <$ 0.46 eV) in three runs, with wave packet energies centered at 0.008, 0.1, and 0.29 eV. For the lowest energy run, the grid extends between ($x = 0.18a_0$, $y = 1.3a_0$, $z = -1.5a_0$) and ($x = 130a_0$, $y = 22a_0$, $z = 1.5a_0$), corresponding to 128 points to cover the L_x range, 32 for the l_x range, 180 for the L_y range, 32 for the l_y range, and 48 in the z direction (see Figure 4 for the definition of the L and l quantities). An efficient absorption requires an absorbing zone as large as $30a_0$ in the x direction, and $10a_0$ in the y direction, and absorption parameters as small as $\beta_x = 4.1\ 10^{-7}$ au and $\beta_y = 8.0\ 10^{-5}$ au.

Just before reaching the large y absorption zone, the reactive part of the wave packet is analyzed by a standard method: the time dependent projections of the wave packet onto the H_2 vibrational eigenstates ζ_v and onto the eigenstates $\xi_{v'}$ of the vibrating coronene molecule

$$c_{vv'}(t) = \int_{z=-\infty}^{\infty}\int_{x'=0}^{\infty} \zeta_v(x')\xi_{v'}(z)\psi(R'^*,x',z,t)\,\mathrm{d}x'\,\mathrm{d}z \tag{18}$$

are analyzed in term of their energy components by a time-to-energy Fourier transform.

$$\tilde{c}_{vv'}(E) = \frac{1}{\sqrt{2\pi}}\int_{-\infty}^{\infty} c_{vv'}(t)\exp\left(\frac{\mathrm{i}Et}{\hbar}\right)\mathrm{d}t \tag{19}$$

In eq 18, R' is the Jacobi coordinate in the product valley:

$$R' = y + \frac{x}{2} \tag{20}$$

Its value R'^* in eq 18 is such that the analysis line is located in the asymptotic zone of the PES, that is, in a region where V does not depend on R'. The reaction probability $P_{\text{rea}}(E,v,v')$

depends on the total energy E and on the vibrational states of the H_2 and coronene molecules according to

$$P_{\mathrm{rea}}(E,v,v') = \frac{\hbar^2 K K'_{vv'}}{2m^2} \frac{|\tilde{c}_{vv'}(E)|^2}{|\tilde{F}(K)|^2} \tag{21}$$

In the above equation, K and $K'_{vv'}$ are related to the total energy E and to the internal energy ϵ of the cor−H(ν_1=ν_2=0) + H or to the internal energy $\epsilon'_{v,v'}$ of the cor(v') + H_2(v) systems by

$$\frac{\hbar^2 K^2}{2m} + \epsilon = E \quad \text{and} \quad \frac{\hbar^2 K'^2_{vv'}}{4m} + \epsilon'_{vv'} = E \tag{22}$$

and $\tilde{F}(K)$is the K component of the Fourier transform of $F(R)$.

The functions $P_{\mathrm{rea}}(E,v,v')$ are the most detailed results provided by this state-to-state calculation. We shall also present some less detailed results, such as the probability to form H_2 in a given v state:

$$P_{\mathrm{H_2}}(E,v) = \sum_{v'} P_{\mathrm{rea}}(E,v,v') \tag{23}$$

or the probability to produce the coronene molecule in a given v' state:

$$P_{\mathrm{cor}}(E,v') = \sum_{v} P_{\mathrm{rea}}(E,v,v') \tag{24}$$

or finally the total reaction probability

$$P_{\mathrm{tot}}(E) = \sum_{vv'} P_{\mathrm{rea}}(E,v,v') \tag{25}$$

For comparison purposes, we have performed a few quasi-classical trajectory calculations (QCT) with the same geometrical constraints to compare classical and quantal results. We have also performed 2D quantal calculations using two different approximations: in the *sudden approximation*, the C* atom is not allowed to move, that is, z is kept fixed at its equilibrium value z_{eq} in the cor−H compound. In the *adiabatic approximation*, the C* atom adiabatically follows the x and y motions. Basically, the equations that govern these 2D calculations are the same. The Hamiltonian is written

$$\hat{\mathbf{H}} = \frac{\hat{p}_x(2\hat{p}_x - \hat{p}_y)}{2m} + \frac{\hat{p}_y(\hat{p}_y - \hat{p}_x)}{2m} + V_{\mathrm{2D}}(x,y) \tag{26}$$

where V_{2D} is

$$V_{\mathrm{2D}}(x,y) = V(x,y,z_{\mathrm{eq}}) \quad \text{(sudden approximation)}$$
$$V_{\mathrm{2D}}(x,y) = \min_z(V(x,y,z)) \quad \text{(adiabatic approximation)} \tag{27}$$

The mapping procedure described in eqs 8−13 has also been applied for the 2D calculations.

4. Results and Discussion

Exact Calculation. The so-called *exact* results refer to the situation where the C* atom in the coronene molecule vibrates. The corresponding reaction probability is shown in Figure 5: it grows at low energy and remains close to 1 as soon as the collision energy is larger than about 25 meV. The same behavior is observed in a quasi-classical trajectory calculation, although the latter obviously fails to reproduce the low-energy behavior. From an astrophysical point of view, this low collision behavior is very important. One can see in Figure 5 that the reaction probability becomes low at low collision energy. It reaches 50% at E_{coll} = 9.3 meV (i.e., at E/k_{B} = 107 K). This is related to the above-mentioned barrier in the entrance channel, which, when taking into account the zero-point energy, is 9.2 meV high. The role of the barrier is demonstrated by the comparison of the exact reaction probability with the prediction of a capture model, where the reaction probability is assumed to be 1 as soon the system overcomes the barrier in the entrance valley. Clearly, the barrier plays a prominent role in the low-energy reaction probability.

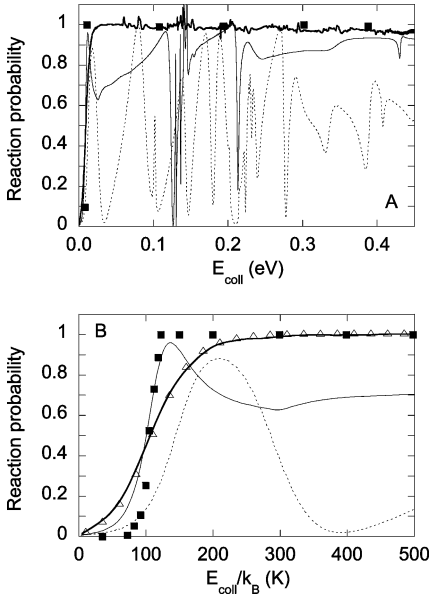

Figure 5. Reaction probability at high collision energy (frame A) or low collision energy (frame B). Bold line: 3D calculation. Thin line: 2D adiabatic approximation. Dotted line: 2D sudden approximation. Squares: QCT calculation. Triangles: capture model.

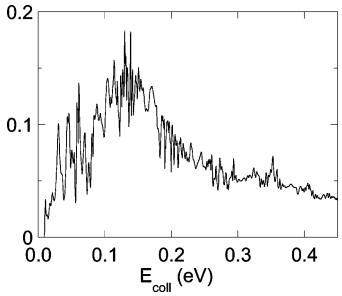

Figure 6. R probability in the coronene(v'=5) + H_2(v=9) channel.

The state-to-state reaction probabilities have a much more complicated energy dependence (Figure 6), and exhibit many complicated structures, which have probably to be related to resonances. Indeed, the time evolution of the wave packet shows that parts of the system can be trapped in the reaction region during about 2 ps. In the considered collision energy range there are always more than 273 open vibrational v,v' states for the H_2(v) + cor(v') system. Therefore, when summing over all contributions, the structures observed in each state-to-state channel are washed out.

The v,v' state-to-state reaction probability is shown in Figure 7 at three different collision energies. The overall shape of the distribution of the products does not depend much on the collision energy. It is seen that the H_2 molecule is formed in its highest energetically allowed vibrational levels. The coronene molecule is comparatively much less excited. The same features can be observed in Figure 8, which shows how the available energy is shared between the internal and external degrees of

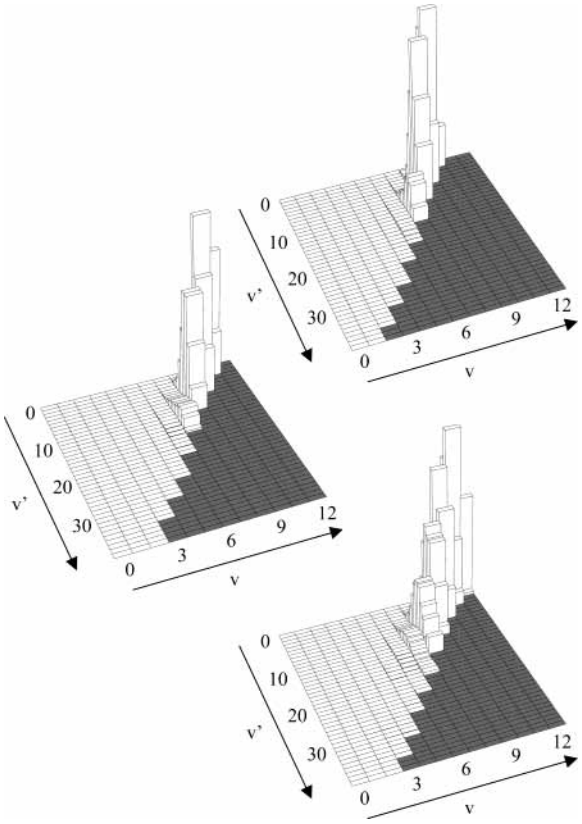

Figure 7. State-to-state reaction probability at $E_{coll} = 0.01$, 0.1, and 0.4 eV from top to bottom. The gray zones correspond to closed channels.

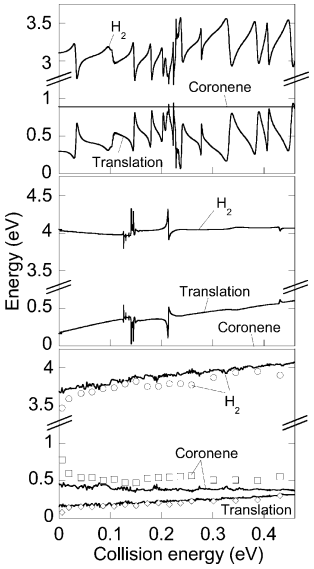

Figure 8. Expectation value of the H_2 internal energy, coronene internal energy, and translation energy. Upper frame: sudden approximation. Middle frame: adiabatic approximation. Lower frame: exact calculation (full line) and QCT calculation (symbols).

freedom of the reaction products. In the whole collision energy range studied here, the main part of the available energy goes into the H_2 vibration, which is excited up to $v = 10$ even at low collision energy (Figure 9). The energy left in the coronene molecule is typically 6 times lower, and the translational energy of the nascent H_2 is even smaller (Figure 8).

Approximate Methods. The results obtained in the *sudden* approximation have been presented elsewhere[22] and will only be summarized here. The total reaction probability smoothly

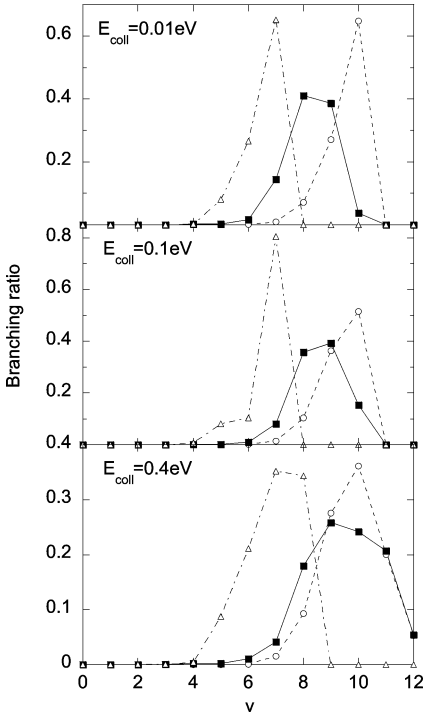

Figure 9. H_2 vibrational distribution at three different collision energies. Full line: 3D calculation. Dashed line: 2D adiabatic approximation. Dot-dashed line: 2D sudden approximation.

oscillates as a function of the collision energy (Figure 5). These oscillations have been attributed to short-lived resonances with lifetimes on the order of a few tens of femtoseconds. Just as in the exact calculation, the reaction probability strongly decreases at low collision energy. Whatever the collision energy is, the H_2 molecule is formed with a substantial internal energy, the most populated level being almost always the highest possible one (Figure 9). The amount of energy left in the coronene molecule is fixed by the sudden approximation, which prevents the C* atom from moving during the collision. The coronene molecule is left with a substantial amount of potential energy. The translational coronene$-H_2$ relative energy is low.

Except for a few regions exhibiting resonances, the energy dependence of the *adiabatic* reaction probability is on the whole rather smooth, except within a few regions where two different types of resonances can be observed. A first type of resonance appears in the collision energy range between 0.12and 0.15 eV. The very sharp structures are associated with very long-lived resonances corresponding to the trapping of the H_2 molecule in its physisorption well (Figure 10). From the time evolution of the outgoing flux, the lifetimes of these very sharp resonances have been estimated to be about 2 ps. Incidentally, it should be mentioned that though the propagation time is as long as 22 ps, our calculation gets in trouble in the regions of these resonances; this is witnessed by the magnitude of the reaction probability which becomes larger than 1 at resonance. Probably, our method is not accurate enough to correctly predict these long time scale phenomena. A second type of resonance is associated with the opening of inelastic channels (cor$-$H(v=1) + H at 0.21 eV, cor$-$H(v=2) + H at 0.43 eV). Just as in the other cases, the H_2 molecule is formed with considerable internal energy (Figure 9). The amount of energy left in the coronene molecule is fixed to zero by the adiabatic approximation. The translational coronene$-H_2$ relative energy is always low.

Discussion. The sudden approximation assumes that the relaxation of the coronene molecule is much slower than the reaction. On the contrary, the adiabatic approximation assumes

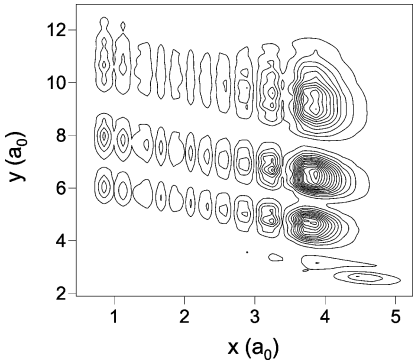

Figure 10. Snapshot of a wave packet obtained in the adiabatic approximation after a propagation time of 2.16 ps. The energy distribution of the initial wave packet is 141 ± 13 meV, i.e., on the third resonant structure observed in Figure 5. The wave packet is still trapped in the physisorption well of the exit valley. The H_2 molecule is in its $v = 10$ vibrational level and is trapped in the second vibrationally excited state of the physisorption well.

that the relaxation of the coronene is much faster than the collision. Actually, the real situation lies somewhere in between. One could thus naively expect that the exact results are somewhat intermediate between the sudden results and the adiabatic results. In fact, this is not the case: the exact reaction probability is almost always larger than those predicted by the approximations. This is especially the case at the very low collision energies (Figure 5) which are of astrophysical interest. At low energy, one may think that the activation barrier is responsible for this behavior. (Notice that the activation barrier is not the same in the exact calculation and in the approximate ones owing to the zero-point energy of the coordinates perpendicular to the reaction coordinate.) Actually, the activation barrier is not the main reason. To show this, we have compared the exact reaction probability with the prediction of a capture model. In the capture model, the reaction probability is the transmission coefficient in one dimension of a particle whose time evolution is governed by the Hamiltonian

$$\hat{\mathbf{H}} = -\frac{\hbar^2}{2m}\frac{\partial^2}{\partial s^2} + V_{\mathrm{MEP}}(s) \qquad (28)$$

where $V_{\mathrm{MEP}}(s)$ is the potential along the minimum energy path shown in Figure 2. One clearly sees in Figure 5 that the capture model nicely fits the exact calculation. Now, the approximate calculations do not behave in that way. We have shown in a previous paper[22] that the sudden reaction probability is about 50% smaller than the prediction of the capture model. This means that the motion of the C* atom makes the reaction easier in the sense that it helps the system turn the corner of the PES in the interaction region. At first sight this result is surprising. Indeed, since the motion of the C* atom in the exact calculation is of relatively small amplitude compared to the motions of the H atoms (Figure 11) one might think that its exact position is of little effect on the reactivity. Actually, the effect of the C* atom motion can presumably be interpreted in a mechanical picture very similar to the role of the umbrella bending motion of the NH_3^+ ion in the reaction[42]

$$NH_3^+ + H_2 \rightarrow NH_4^+ + H \qquad (29)$$

Very simply, the point is that the strength of the bond between the chemisorbed H atom and the C* atom is very sensitive to the distance between C* and the coronene plane. Indeed, the DFT calculation[26,27] of the cor−H system has shown that a C* atom in the coronene plane is not chemically attractive for the H atom, while it becomes attractive when it moves out of the plane toward the H atom. This is probably related to the change in the hybridization state of the C* atom from sp^2 in the coronene plane to sp^3 out of that plane. Then, as the C* atom in the exact calculation moves very quickly toward the coronene plane, and even explores negative z abscissas, the C*−H bond is likely to become very weak in the exact calculation, and even weaker than in the adiabatic one. Considering actual H−H− grain interactions in the IMS, the discussed effect is probably less pronounced when taking into account the dissipation of the vibration energy of the C* atom into the grain. Nevertheless, we have checked on a rough classical calculation based upon the Brenner II model potential[43] that the dumping of the C atom vibration is not as fast as the reaction studied here.

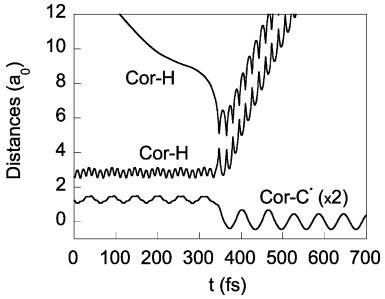

Figure 11. Time evolution of the distances of the three atoms with respect to the coronene plane during the reaction in a classical calculation. The collision energy is 0.011 eV. One clearly sees that the C* atom moves from one side of the coronene plane to the opposite side during the reaction.

The results concerning the energy sharing between the three degrees of freedom after the reaction (Figure 8) are less surprising. All three calculations predict that the translational energy is low. By construction, a significant amount of energy (0.89 eV) has to be left in the coronene molecule in the sudden approximation, while this energy is 0 in the adiabatic approximation. The exact calculation predicts that this energy is about 0.4 eV, which is intermediate between the two approximations. When looking at the H_2 internal state distribution (Figure 9), one also finds that the exact calculation gives intermediate results between the sudden and the adiabatic approximations.

Comparison with Previous Studies. As mentioned in the Introduction, a number of recent works have been devoted to the study of H_2 formation on graphite through the ER mechanism. A first comparison can be made with the quantal study of Sha et al.,[21] which was not restricted to the collinear geometry but which does not handle the surface relaxation effects. Like in the present work, they find that the reaction is easier in the adiabatic approximation than in the sudden approximation. At moderate collision energy ($E_{\mathrm{coll}} < 0.1$ eV), the H_2 vibrational energy they find, although slightly smaller than ours (Figure 8), is also very high: at $E_{\mathrm{coll}} = 30$ meV, $\langle v \rangle \approx 5.5$ in the sudden approximation, and $\langle v \rangle \approx 8$ in the adiabatic approximation. At collision energies larger than 0.2 eV, they find that the rotation energy becomes more important, which of course we cannot guess. Nevertheless, the translational energy always remains small.

A second comparison can be made with the work of Rutigliano et al.,[17] to which Gert Billing contributed. The approach they used differs from ours in many points. First, the motion of the H atoms is handled classically, while the coupling to the crystal phonons is handled quantally. Second, the PES they use is not the same as ours, although both PESs have strong

similarities. Notwithstanding these differences, their results are very close to the present ones. The collision energy dependence of the reaction probability they find increases from 0 at $E_{coll} = 0$ to about 1 when $E_{coll} \approx 0.04$ eV, reaching 50% at $E_{coll} \approx 0.01$ eV, which is very close to the present findings. On the other hand, the product energy distribution of Rutigliano et al.[17] at E_{coll} below 0.1 eV is typically 10% in the surface heating, 20% in the translational energy, and 70% in the H_2 internal energy. As seen on Figure 8, these numbers are in reasonable agreement with our results. In particular, we agree on the fraction of energy left in the grain.

At present, comparison with experiment is far from being straightforward. Indeed, we have restricted ourselves to the study of the ER mechanism on a coronene molecule, similar to a graphite monocrystal with very low H coverage. In the experiments, both ER and LH mechanisms can of course take place. Moreover, in the experiments, the surface is probably significantly covered by adsorbed H atoms. The available experimental results do not show as large a vibrational excitation energy as evidenced in the present work. Yet, vibrationally excited nascent H_2 has been observed in the $v = 1$ level.[44] This discrepancy could be related to the effect of the surface coverage by H atoms, which has been recently shown to decrease the H_2 vibrational excitation.[45]

5. Conclusion

We have presented a time dependent quantal study of the dynamics of the H_2 formation through a collinear ER mechanism which explicitly handles substrate relaxation effects. Our substrate is a PAH which exhibits some strong similarity with a perfect graphite (0001) surface. This study has been undertaken down to very low collision energy ($T = 5$ K). This has been made possible by the combined use of an L-shaped grid and of the very efficient mapping procedure introduced by Borisov.[39]

The reaction probability is governed by a small activation barrier, which at low collision energy partially prevents the system from entering the interaction region. Nevertheless, as soon as the system enters this region, the reaction takes place: the collinear reaction strictly follows the prediction of a capture model. Most of the available energy goes into the H_2 vibration, which is excited typically to $v = 8$. The excitation of the coronene molecule is typically 8 to 10 times smaller, and the translation energy is even smaller.

To avoid handling the surface relaxation effects, both the sudden approximation and the adiabatic approximation have been used in previous studies on this system. The present work shows that, at least in the collinear geometry, the adiabatic approximation is much better. Nevertheless, it is far from being perfect, for three reasons: (i) it cannot predict the amount of energy left in the surface, (ii) it predicts an H_2 excitation that is too large, and (iii) it strongly underestimates the reaction probability below 50 K.

Finally, one may recall that the reaction studied here is but the second step in the H_2 production scenario in the ISM, the first one being the chemisorption of an H atom. There is a 0.25 eV activation barrier for that chemisorption[27] which is very difficult to overcome in ISM conditions. Therefore, it is possible that H chemisorption constitutes a bottleneck for the total reaction. However, two effects have to be taken into account to estimate the relative rates of the two steps. First, because the grain is a macroscopic object, an H−grain collision is much more likely to occur than the collision of an H atom coming from the gas phase with an H atom already chemisorbed on the grain. Second, the chemisorption probability could be enhanced if the H atom is first physisorbed, which is probably very easy in the ISM conditions. It would then tunnel through the barrier in an excited state of the chemisorption well and finally relax in the chemisorption ground state. This process, which is still open to investigation, is undoubtedly very slow compared to the time scale of the title reaction, still it could be very fast compared to the time scales of the chemical evolution of interstellar clouds.

Acknowledgment. The authors thank Guillaume Pineau des Forêts for fruitful discussions. They also acknowledge the program "Physico Chimie du Milieu Interstellaire" for financial support.

References and Notes

(1) Hollenbach, D. H.; Salpeter, E. E. *Astrophys. J.* **1971**, *163*, 155.
(2) Le Bourlot, J.; Pineau des Forêts, G.; Roueff, E.; Dalgarno, A.; Gredel, R. *Astrophys. J.* **1995**, *449*, 178.
(3) Burton, M. G.; Bulmer, M.; Moorhouse, A.; Geballe, T. R.; Brand, P. W. J. L. *Mon. Not. R. Astron. Soc.* **1992**, *257*, 1.
(4) Gough, S.; Schermann, C.; Pichou, F.; Landau, M.; Čadež, I.; Hall, R. I. *Astron. Astrophys.* **1996**, *305*, 687.
(5) Pirronello, V.; Biham, O.; Liu, C.; Shen, L.; Vidali, G. *Astrophys. J.* **1997**, *475*, L69.
(6) Pirronello, V.; Biham, O.; Liu, C.; Shen, L.; Vidali, G. *Astrophys. J.* **1997**, *483*, L131.
(7) Vidali, G.; Pirronello, V.; Liu, C.; Shen, L. *Astrophys. Lett.* **1998**, *35*, 423.
(8) Pirronello, V.; Liu, C.; Roser, J. E.; Vidali, G. *Astron. Astrophys.* **1999**, *344*, 681.
(9) Perry, J. S. A.; Gingell, J. M.; Newson, K. A.; To, J.; Watanabe, N.; Price, S. D. *Meas. Sci. Technol.* **2002**, *13*, 1414.
(10) Biham, O.; Furman, I.; Katz, N.; Pirronello, V.; Vidali, G. *Mon. Not. R. Astron. Soc.* **1998**, *296*, 869.
(11) Katz, N.; Furman, I.; Biham, O.; Pirronello, V.; Vidali, G. *Astrophys. J.* **1999**, *522*, 305.
(12) Cazaux, S.; Tielens, C. G. M. *Astrophys. J.* **2002**, *575*, L29.
(13) Parneix, P.; Bréchignac, P. *Astron. Astrophys.* **1998**, *334*, 363.
(14) Kim, Y. H.; Ree, J.; Shin, H. K. *Chem. Phys. Lett.* **1999**, *314*, 1.
(15) Farebrother, A. J.; Meijer, A. J. H. M.; Clary, D. C.; Fisher, A. J. *Chem. Phys. Lett.* **2000**, *319*, 303.
(16) Meijer, A. J. H. M.; Farebrother, A. J.; Clary, D. C.; Fisher, A. J. *J. Phys. Chem. A* **2001**, *105*, 2173.
(17) Rutigliano, M.; Cacciatore, M.; Billing, G. D. *Chem. Phys. Lett.* **2001**, *340*, 13.
(18) Jackson, B.; Lemoine, D. *J. Chem. Phys.* **2001**, *114*, 474.
(19) Ree, J.; Kim, Y. H.; Shin, H. K. *Chem. Phys. Lett.* **2002**, *353*, 368.
(20) Sha, X.; Jackson, B. *Surf. Sci.* **2002**, *496*, 318.
(21) Sha, X.; Jackson, B.; Lemoine, D. *J. Chem. Phys.* **2002**, *116*, 7158.
(22) Morisset, S.; Aguillon, F.; Sizun, M.; Sidis, V. *Phys. Chem. Chem. Phys.* **2003**, *5*, 506.
(23) Morisset, S.; Aguillon, F.; Sizun, M.; Sidis, V. *Chem. Phys. Lett.* **2003**, *378*, 615.
(24) Mathis, J. S.; Rumpl, W.; Nordsiek, K. H. *Astrophys. J.* **1977**, *217*, 425.
(25) Fitzpatrick, E. L.; Massa, D. *Astrophys. J.* **1990**, *72*, 163.
(26) Jeloaica, L.; Sidis, V. *Chem. Phys. Lett.* **1999**, *300*, 157.
(27) (a) Sidis, V.; Jeloaica, L.; Borisov, A. G.; Deutscher, S. A. In *Molecular Hydrogen in Space*; Combes, F., Pineau des Forêts, G., Eds; Cambridge Contemporary Astrophysics Series; Cambridge University Press: Cambridge, U.K.; New York, 2000; pp 89−97. (b) Jeloaica, L.; Sidis, V. In *DFT 2001*, Proceedings of the 9th International Conference on the Applications of the Density Functional Theory in Chemistry and Physics, SL de El Escorial, Madrid; 2001; p 201.
(28) (a) Jacobson, N. M.Sc. Thesis, Göteborg University, Göteborg, Sweden, 2000. (b) Jacobson, N.; Tegner, B.; Schröder, E.; Hyldgaard, P.; Lundqvist, B. I. *Comput. Mater. Sci.* **2002**, *24*, 273.
(29) Jacobson, N. Private communication.
(30) Ferro, Y.; Marinelli, F.; Allouche, A. *J. Chem. Phys.* **2002**, *116*, 8124; *Chem. Phys. Lett.* **2003**, *368*, 609.
(31) (a) Baerends, E. J.; Ellis, E. D.; Ros, P. *Chem. Phys.* **1973**, *2*, 41. (b) Te Velde, G.; Baerends, E. J. *J. Comput. Phys.* **1992**, *99*, 84.
(32) Vosko, S. H.; Wilks, L. H.; Nussair, M. *Can. J. Phys.* **1980**, *58*, 1200.
(33) Wang, Y.; Perdew, J. P. *Phys. Rev. B* **1991**, *43*, 8911.
(34) (a) Fukui, K. *Acc. Chem. Res.* **1981**, *14*, 363. (b) Page, M.; McIver, J. W., Jr. *J. Chem. Phys.* **1988**, *88*, 922.

(35) Mowrey, R. C. *J. Chem. Phys.* **1991**, *94*, 7098.
(36) Kosloff, R. In *Time Dependent Quantum Molecular Dynamics*; NATO ASI Series, Series B: Physics; Broekhove, J., Lathouvers, L., Eds.; Plenum: New York, 1992; Vol. 299, p 97.
(37) Kokoouline, V.; Dulieu, O.; Kosloff, R.; Masnou-Seeuws, F. *J. Chem. Phys.* **1999**, *110*, 9865.
(38) Lemoine, D. *Chem. Phys. Lett.* **2000**, *320*, 492.
(39) Borisov, A. G. *J. Chem. Phys.* **2001**, *114*, 7770.
(40) Kosloff, D.; Kosloff, R. *J. Comput. Phys.* **1983**, *52*, 35.
(41) Leforestier, C.; Bisseling, R. H.; Cerjan, C.; Feit, M. D.; Friesner, R.; Guldberg, A.; Hammerich, A.; Jolicard, G.; Karrlein, W.; Meyer, H-D.; Lipkin, N.; Roncero, O.; Kosloff, R. *J. Comput. Phys.* **1991**, *94*, 59.
(42) Aguillon, F.; Sizun, M. *J. Chem. Phys.* **2000**, *112*, 10179.
(43) Brenner, D. W. *Phys. Rev. B* **1990**, *42*, 9458.
(44) Perry, J. S. A.; Gingell, J. M.; Newson, K. A.; To, J.; Watanabe, N.; Price, S. D. *Meas. Sci. Technol.* **2002**, *13*, 1414.
(45) Meijer, A. J. H. M.; Fisher, A. J.; Clary, D. C. *J. Phys. Chem. A* **2003**, *107*, 10862.